Direct Determination of Fission-Barrier Heights using Light-Ion Transfer in Inverse Kinematics

S. A. Bennett,[1] K. Garrett,[1] D. K. Sharp,[1,*] S. J. Freeman,[1,2] A. G. Smith,[1] T. J. Wright,[1] B. P. Kay,[3] T. L. Tang,[3,†] I. A. Tolstukhin,[3] Y. Ayyad,[4] J. Chen,[3] P. J. Davies,[5] A. Dolan,[6] L. P. Gaffney,[6] A. Heinz,[7] C. R. Hoffman,[3] C. Müller-Gatermann,[3] R. D. Page,[6] and G. L. Wilson[8,3]

[1]*Department of Physics and Astronomy, University of Manchester, Manchester M13 9PL, United Kingdom*
[2]*CERN, CH-1211 Geneva 23, Switzerland*
[3]*Physics Division, Argonne National Laboratory, Lemont, Illinois 60439, USA*
[4]*IGFAE, Universidade de Santiago de Compostela, E-15782 Santiago de Compostela, Spain*
[5]*School of Physics, Engineering and Technology, University of York, Heslington, York YO10 5DD, United Kingdom*
[6]*Oliver Lodge Laboratory, University of Liverpool, Liverpool L69 7ZE, United Kingdom*
[7]*Chalmers University of Technology, SE-41296 Göteborg, Sweden*
[8]*Louisiana State University, Baton Rouge, Louisiana 70803, USA*

(Dated: February 28, 2023)

We demonstrate a new technique for obtaining fission data for nuclei away from β-stability. These types of data are pertinent to the astrophysical r-process, crucial to a complete understanding of the origin of the heavy elements, and for developing a predictive model of fission. These data are also important considerations for terrestrial applications related to power generation and safeguarding. Experimentally, such data are scarce due to the difficulties in producing the actinide targets of interest. The solenoidal-spectrometer technique, commonly used to study nucleon-transfer reactions in inverse kinematics, has been applied to the case of transfer-induced fission as a means to deduce the fission-barrier height, among other variables. The fission-barrier height of ^{239}U has been determined via the ^{238}U(d,pf) reaction in inverse kinematics, the results of which are consistent with existing neutron-induced fission data indicating the validity of the technique.

The majority of heavy nuclei, including those important in both terrestrial and astrophysical settings, have no available nuclear data from neutron-induced fission [1]. For example, the astrophysical r-process is thought to account for the creation of approximately half of the heavy elements beyond iron. Alongside other ingredients, fission data such as barrier height and mass and charge yields are crucial inputs in performing accurate abundance calculations for high-Z nuclides [2–4]. In particular, the so-called fission recycling mechanism defines the upper mass limit in the r-process, and channels mass to lower regions of the nuclear chart, thus contributing to the abundances of medium mass nuclei. Moreover, in the era of multi-messenger astronomy, fission data are critical for a deeper understanding of results which suggest that fission is significant in the process of nucleosynthesis in neutron-star mergers [3]. For example, the fission product ^{90}Sr has recently been observed in the remnants of such an event [5].

Current benchmarking of fission models is performed indirectly, for example by comparing the limits of the neutron capture process in nuclear explosions to those predicted in calculations [6]. Validating these models for the case of nuclei with short half-lives is not feasible due to the impracticability of producing fixed targets. For direct validation, alternative methods are required, for example by using the fissioning system as a beam to obtain experimental data. Furthermore the benchmarking of fission models [6–8] and collection of fission data for short-lived actinides, including fission barriers and mass and charge yields, are key quantities for future terrestrial power and safeguarding applications [9, 10].

Any reaction where the Q value can be accurately determined and that produces the excited compound system of interest can be used to probe the fission barrier. Direct reactions can, for example, be used to populate single-particle doorway states leading to compound nucleus formation. In the (d,p) reaction, the neutron transferred from the deuteron to the target nucleus acts as a proxy for the neutron-induced reaction. By studying the (d,pf) reaction, information can be obtained about the fission-barrier height. The probability of fission and the neutron-induced fission cross section can also be deduced, assuming that the fission cross section σ_{f}^{A} can be factorised into a compound nucleus formation cross section $\sigma_{\mathrm{CN}}^{A+1}$ and fission decay probability P_{f}^{A+1}:

$$\sigma_{\mathrm{f}}^{A} = \sigma_{\mathrm{CN}}^{A+1} \times P_{\mathrm{f}}^{A+1}. \quad (1)$$

The technique was first demonstrated in normal kinematics by Northrop *et al.* [11] and by Cramer and Britt [12], where the fixed target was the actinide species of interest.

There are numerous examples of reaction-induced fission experiments from which the fission-barrier height, fission probability, and other properties such as mass split have been accurately deduced. In normal kinematics, examples include: (d,pf) [13, 14], (t,pf) [12, 14], (^{3}He,αf) [15], and in inverse kinematics: (^{9}Be,^{8}Be f) [16, 17] and multinucleon transfer [17–19]. A review of the

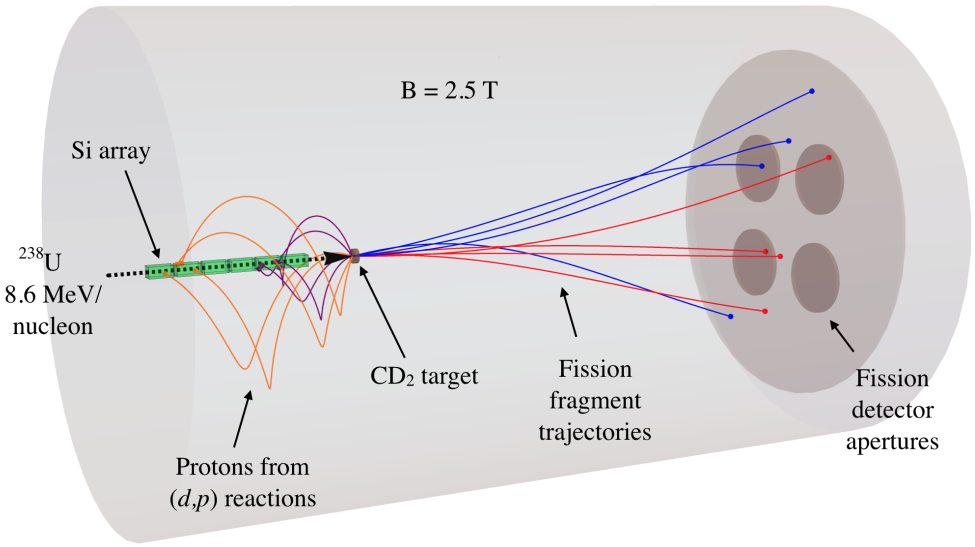

FIG. 1. To-scale schematic of the experimental setup with example particle trajectories for ^{238}U(d,pf) events. Example proton trajectories for reactions populating the ground state in ^{239}U (orange curves) and states at 7 MeV close to the fission barrier (purple curves) are shown for a range of c.m. proton angles. Example fission fragment trajectories are also shown for fragments with $A = 138$ (red curves) and $A = 100$ (blue curves), for a range of emission angles. The equally spaced circular detector apertures have radius 8 cm, and are centred 18 cm from the beam axis. The axial distance between the target and detector apertures is 70 cm.

technique can be found in Ref. [20], where questions around the degree to which direct reactions can act as true "surrogates" for neutron-induced compound reactions are also discussed. For example, in near-barrier fission, the low level density leads to a strong sensitivity of the fission probability to the spin-parity distribution of states populated in the transfer reaction, which are plausibly very different to those of neutron-induced reactions [21, 22]. In general however, results compare remarkably well with neutron-induced data.

In this work, we present a study of the transfer-induced fission of ^{239}U in inverse kinematics with the (d,pf) reaction using the solenoidal-spectrometer technique. This is presented as an an exploratory case where there are existing fission data, and constitutes the first direct measurement of a fission-barrier height using a light-ion transfer reaction in inverse kinematics. Experiments performed in such a way, using unstable species as a beam, clearly permit studies of a large number of nuclei that are not accessible in fixed-target experiments in normal kinematics, nor by using multinucleon transfer on stable beams in inverse kinematics. There exist three solenoidal spectrometers used for transfer reaction studies: HELIOS at Argonne National Laboratory (ANL) [23], the ISOLDE Solenoidal Spectrometer at CERN [24], and SOLARIS at FRIB [25]. There are many available radioactive beams of sufficient intensity at the facilities hosting such devices to which the method presented in this paper may be applied. In the longer term, it is envisaged that more exotic, neutron-rich isotopes will become available with developments at these facilities, for example ReA (FRIB) [26], and the LISA project in Europe (ISOLDE) [27].

The experiment was carried out using HELIOS at ANL. The geometry is shown in Fig. 1, along with the calculated trajectories of reaction products. Light ions emitted following reactions of the beam with a deuterated polyethylene (CD_2) target are transported to a four-sided position-sensitive silicon array situated upstream of the target surrounding the beam axis, which is itself collinear with a solenoidal magnetic field. The Si array is used to measure the laboratory energy of light ejectiles and their return distance to the beam axis. The 350-mm long Si array was positioned such that the end was 55 mm upstream of the target. In this configuration protons from (d,p) reactions populating states at an excitation energy of 7 MeV emitted at angles from approximately 10° to 30° in the center-of-mass frame (c.m.) hit the array. The Si array was calibrated in energy using α particles from a ^{228}Th source. Downstream of the target, a Faraday cup (not shown in Fig. 1) was used to measure beam current, and an annular silicon detector was used to detect elastically scattered deuterons for a narrow range of c.m. angles between 29° and 29.3°. The latter allows an absolute normalisation of measured yields to generate absolute cross sections.

A set of gas-filled heavy-ion detectors was used downstream of the target to study the subset of residual ^{239}U nuclei that fission. In inverse kinematics, the fission-fragment angular distribution is strongly forward peaked in the laboratory as indicated by the example

trajectories shown in Fig. 1. With a beam energy of 8.6 MeV/nucleon, light and heavy fragments from the fission of actinide nuclei form two cones at laboratory angles of approximately 15° and 10° respectively. An aluminium charge-reset foil with a thickness of 100 μg/cm^2 was positioned 70 mm downstream of the target in order to minimise the spread of charge states of fission fragments emitted at different depths inside the CD_2 target. Four fission detection arms were positioned around 1 m downstream of the target, two at 15° to the beam axis and two at 10° to maximise the acceptance of light and heavy fragments. Each of the arms had a position-sensitive multi-wire proportional counter (MWPC) followed by a gaseous axially-segmented Bragg detector. On an event-by-event basis, the Bragg detector yielded the total and specific energy-loss of any detected fragments, and the MWPCs gave their position at the entrance to the Bragg detectors. The position was internally calibrated using the α particles from the ^{228}Th source. The MWPCs were also used to generate a precise timing signal used to correlate fission fragments to Si array events. The intrinsic efficiency was close to 100%. The geometric efficiency was ∼10% for the detection of one or more fission fragments, and ∼1% for the coincident detection of light and heavy fragments (more details below). The energy loss for typical light on the efficiency considerations for the fission fragment detectors. On an event-by-event basis, the information yielded by the fission detectors is sufficient to deduce the fission mass split and c.m. fission axis orientation, through kinematic reconstruction, and the atomic number of each fragment using Bragg-peak spectroscopy [28]. These capabilities allow for the simultaneous measurement of fission yields with excitation energy and fission probability, and will be reported in a future publication.

Placing the Si array upstream of the target and fission fragment detectors downstream leads to precise selection of transfer-induced fission events. With this arrangement, background events such as fission preceded by the evaporation of light charged particles from compound systems is suppressed. To travel into the backwards hemisphere, evaporated particles must possess a large c.m. energy at least as large as the c.m. energy of the beam, around 10 MeV/nucleon here.

A beam of $^{238}U^{47+}$ at an energy of 2.05 GeV (8.6 MeV/nucleon) was delivered by the ATLAS accelerator. The average beam intensity was $\sim 10^6$ pps, with a total integrated beam dose of around 5.5 $\times 10^{11}$ ions. In this time, around 3.5 $\times 10^5$ (d,p) events were detected with the Si array, and around 1000 (d,pf) events were recorded. Due to target damage from the heavy beam, 11 CD_2 targets were used during the experiment with thicknesses between 410 and 590 μg/cm^2. Data were also collected with a pure ^{nat}C target (thickness 584 μg/cm^2) to evaluate backgrounds arising from multinucleon transfer-induced fission reactions on carbon in the CD_2 target [19]. A 2.5-T magnetic field was used, and the digital data acquisition was triggered either by signals in the Si array or any of the MWPCs.

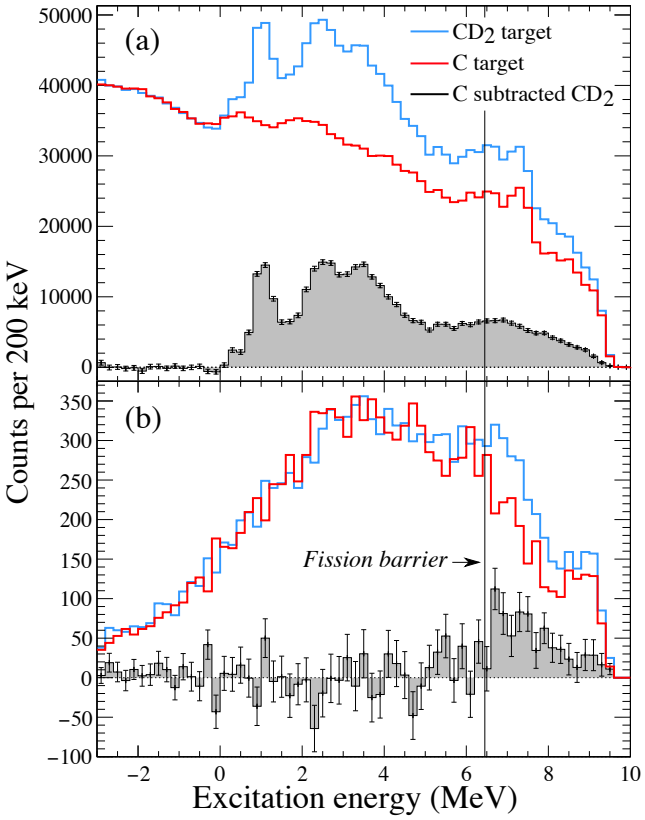

FIG. 2. (a) Excitation-energy spectra associated with all events for Si array data taken with both CD_2 and C targets where the C data has been scaled onto the CD_2 data, and for the carbon subtracted CD_2 data. (b) Same as for (a), but for events in which ≥ 1 fission fragments are detected with the MWPCs of the fission array. The vertical solid line denotes the known fission-barrier height [30]. The carbon target spectra were scaled by ×1.92 and ×1.76 for the singles and fission-gated data, respectively.

Q-value spectra were generated with the measurements of the charged particles detected in the Si array. The Q value was deduced by calculating the c.m. energy of the light ejectile, which itself depends linearly on the laboratory energy and axial return distance to the beam axis [29]. Coincidence events between the Si array and fission detectors were generated by applying a 250-ns wide gate on array-MWPC timing signals. Q-value spectra are shown in Fig. 2. The position of the Si array and a lower energy threshold of 0.5 MeV restricted the measurement to residual nuclei with excitation energy less than around 9.6 MeV. The Q-value resolution was around 250 keV (FWHM). An unresolved multiplet of excited states in ^{239}U around 1 MeV is visible, beyond which there is a continuum. The carbon content of the CD_2 target led to a significant background in both the singles and fission-

gated spectra. It is likely that this background is due to multinucleon transfer-induced fission reactions where light ejectiles intercept the Si array. This background was addressed by evaluating its shape using the data taken with the pure C target. The resulting carbon spectra were scaled to match the spectra obtained with the CD_2 target in the region below the ground state, and subtracted as shown in Fig. 2. Although it might be expected that the carbon target scaling factor for array singles and fission-gated data are similar, the scaling was done separately for each case as the respective factors were found to be different. This suggests the presence of an additional contribution to the array singles data beyond (d,p) reactions, most likely deuteron breakup (see discussion below). For array singles, the data were scaled by normalising over the region $-3 \leq E_x \leq -0.5$ MeV, and for the fission-gated data between $-3 \leq E_x \leq 2$ MeV. The background of time-random Si array-MWPC coincidences was constant with excitation energy, and constitutes 0.43% of the coincident events within the 250-ns time window.

The fission-barrier height was deduced by constructing the fission probability as a function of excitation energy. The probability P_f for the residual nucleus of excitation energy E_x to decay via fission was determined by the ratio

$$P_f(E_x) = \frac{N_{d,pf}(E_x)}{N_{d,p}(E_x) \cdot \epsilon_f} \qquad (2)$$

where $N_{d,pf}(E_x)$ is the number of (d,p) events in coincidence with the detection $\geq$1 fission fragments and $N_{d,p}(E_x)$ is the total number of (d,p) events. The efficiency for the detection of protons from (d,p) events cancels in the ratio, but the fission detection efficiency ϵ_f must be taken into account for a proper normalisation. This was derived from a simulation accounting for the reaction kinematics, geometry, ion transport in the solenoidal magnetic field, and average charge state distributions of the fission fragments. Fission-fragment A and Z yields and average kinetic energy distributions were taken from GEF [31], and the fission axis was assumed to be oriented isotropically in the c.m. frame.

The deduced fission probability is shown in Figure 3. The data taken with both target materials were statistically limited, however an increase in the fission probability between 6 and 7 MeV corresponding to the region around the known fission barrier ($B_f = 6.46$ MeV [30]) is unambiguous and is consistent with the fission barrier deduced from neutron-induced fission data evaluations, also illustrated in Figure 3. This is corroborated with a fit of a Hill-Wheeler function of the form $P_f(E_x) = A \times \{1 + \exp(\frac{2\pi}{\hbar\omega}[B_f - E_x])\}^{-1}$. The parameter A represents the fission probability above the barrier, $\hbar\omega$ is the diffuseness of the barrier and B_f is the height of the fission barrier. For the fit to our data, the diffuseness was fixed taking the value from Ref. [30]

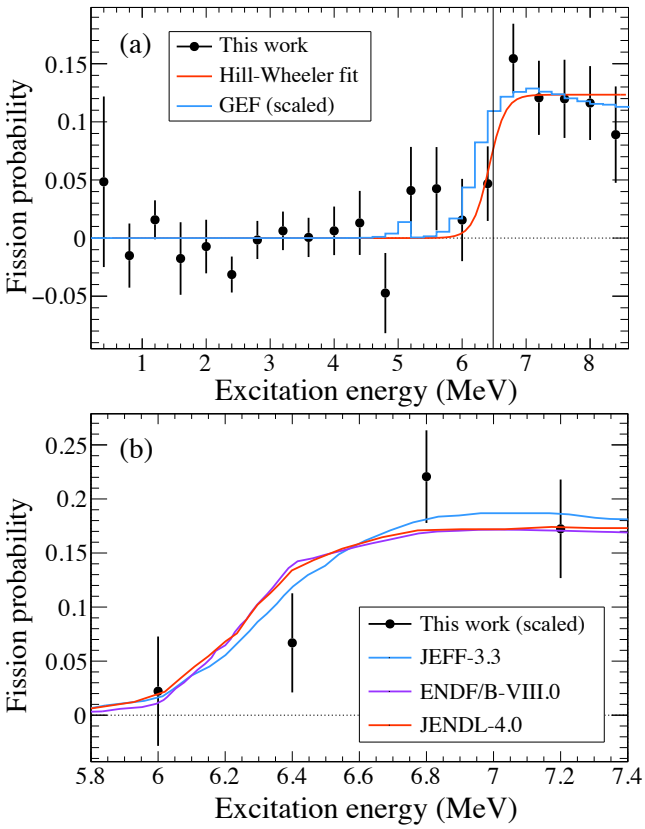

FIG. 3. (a) Experimental fission probability, as defined in Equation 2 compared to a GEF simulation [31] (the GEF result has been normalised to our data) and empirical Hill-Wheeler fit with $\chi^2_{\text{red.}} = 0.57$. The vertical line denotes the known fission-barrier height. (b) Experimental fission probability in the region around the fission barrier compared to probabilities deduced from evaluated nuclear data libraries (JEFF-3.3 [32], ENDF/B-VIII.0 [33], JENDL-4.0 [34]). In the bottom panel, the experimental data have been increased by 30% as explained in the main text. The error bars represent the statistical uncertainty.

($\hbar\omega = 0.8$ MeV), due to a lack of data points defining the region around the barrier. The barrier height in this fitting procedure is, however, largely independent of the diffuseness. The fit gave values of $A = 0.123(15)$ and $B_f = 6.42(12)$ MeV, consistent with the value of $B_f = 6.46$ MeV from Ref. [30]. The shape of the measured fission probability is consistent with the fission probability from GEF [31] as well as data evaluations [32–34]. The absolute magnitude of the fission probability above the barrier is found to be lower than data evaluations by around 30%. This effect, at the same order of magnitude, has been observed in similar studies in normal kinematics [13] and is attributed to deuteron breakup. Protons from breakup reactions lead to a surplus of Si array events and, if not accounted for, are interpreted as being (d,p) events. This leads to an underestimation of the fission probability. The magnitude of

this effect cannot be experimentally determined; theoretical calculations are required to obtain correction factors, see for example Ref. [13]. A further effect, on the level of a few percent, is the angular anisotropy of the fission axis in the c.m. frame which in principle affects the fission-fragment detection efficiency ϵ_f, see for example Ref. [35]. Both corrections, deuteron breakup and fission anisotropy, are not required to extract a value for the fission-barrier height reported in this work. The (d,p) and (d,pf) cross sections are available as Supplemental Material [36].

In conclusion, a fission-barrier height has for the first time been determined using a light-ion transfer reaction in inverse kinematics, in this work for the case of ^{239}U using the solenoidal spectrometer technique, thus unambiguously demonstrating the validity of a technique that can be applied to other cases of interest. By performing similar experiments at the radioactive ion beam facilities with solenoidal spectrometers, this technique could be used to address the scarcity of fission data for a range of short-lived nuclei. Such data are required to benchmark and assess the validity of fission models pertinent to the astrophysical r-process and, in particular, the so-called fission recycling mechanism. It is envisaged that studies of this nature are therefore of fundamental importance to a complete understanding of the origins of the heavy elements, as well as being a powerful tool for gathering nuclear data relevant to terrestrial applications.

Acknowledgements.— This work was supported by the UK Science and Technology Facilities Council under Grant Numbers ST/P004598/1 and ST/V001027/1 (Liverpool), ST/P004423/1 and ST/V001116/1 (Manchester), ST/R004056/1 (Gaffney), ST/T004797/1 (Sharp), ST/N00244X/1 (UK Nuclear Data Network), by the Knut and Alice Wallenberg Foundation Dnr. KAW 2020.0076, and by the U.S. Department of Energy, Office of Science, Office of Nuclear Physics, under Contract Numbers DE-AC02-06CH11357. This research used resources of ANL's ATLAS facility, which is a DOE Office of Science User Facility. The authors would like to acknowledge the support of the ATLAS operations team in the development and delivery of the beam. The open-access experimental data are available at Ref. [37].

* Correspondence to: david.sharp@manchester.ac.uk
† Current address: Department of Physics, Florida State University, Tallahassee, Florida 32306, USA

[1] K.-H. Schmidt and B. Jurado, Review on the progress in nuclear fission — experimental methods and theoretical descriptions, Reports on Progress in Physics **81**, 106301 (2018).
[2] S. A. Giuliani, G. Martínez-Pinedo, M.-R. Wu and L. M. Robledo, Fission and the r-process nucleosynthesis of translead nuclei in neutron star mergers, Phys. Rev. C **102**, 045804 (2020).
[3] S. Goriely, The fundamental role of fission during r-process nucleosynthesis in neutron star mergers, Eur. Phys. J A **51**, 1 (2015).
[4] M. Mumpower, R. Surman, G. C. McLaughlin and A. Aprahamian, The impact of individual nuclear properties on r-process nucleosynthesis, Progress in Particle and Nuclear Physics **86**, 86 (2016).
[5] D. Watson, C. J. Hansen, J. Selsing, A. Koch, D. B. Malesani, A. C. Andersen, J. P. U. Fynbo, A. Arcones, A. Bauswein, S. Covino, A. Grado, K. E. Heintz, L. Hunt, C. Kouveliotou, G. Leloudas, A. J. Levan, P. Mazzali and E. Pian, Identification of strontium in the merger of two neutron stars, Nature (London) **574**, 497 (2019).
[6] P. Möller, A. J. Sierk, T. Ichikawa, A. Iwamoto and M. Mumpower, Fission barriers at the end of the chart of the nuclides, Phys. Rev. C **91**, 024310 (2015).
[7] P. Möller, A. J. Sierk, T. Ichikawa, A. Iwamoto, R. Bengtsson, H. Uhrenholt and S. Åberg, Heavy-element fission barriers, Phys. Rev. C **79**, 064304 (2009).
[8] J. Erler, K. Langanke, H. P. Loens, G. Martínez-Pinedo and P.-G. Reinhard, Fission properties for r-process nuclei, Phys. Rev. C **85**, 025802 (2012).
[9] K. Kolos, V. Sobes, R. Vogt, C. E. Romano, M. S. Smith, L. A. Bernstein, D. A. Brown, M. T. Burkey, Y. Danon and M. A. Elsawi, Current nuclear data needs for applications, Phys. Rev. Research **4**, 021001 (2022).
[10] F. Farget, M. Caamaño, D. Ramos, C. Rodríguez-Tajes, K.-H. Schmidt, L. Audouin, J. Benlliure, E. Casarejos, E. Clément and D. Cortina, Transfer-induced fission in inverse kinematics: Impact on experimental and evaluated nuclear data bases, Eur. Phys. J A **51**, 12 (2015).
[11] J. A. Northrop, R. H. Stokes and K. Boyer, Measurement of the fission thresholds of ^{239}Pu, ^{233}U, ^{235}U, and ^{238}U using the (d,p) reaction, Phys. Rev. **115**, 1277 (1959).
[12] J. D. Cramer and H. C. Britt, Fission studies of thorium, uranium, and plutonium isotopes with (t,pf) reactions, Phys. Rev. C **2**, 2350 (1970).
[13] Q. Ducasse, B. Jurado, M. Aïche, P. Marini, L. Mathieu, A. Görgen, M. Guttormsen, A. C. Larsen, T. Tornyi, J. N. Wilson, G. Barreau, G. Boutoux, S. Czajkowski, F. Giacoppo, F. Gunsing, T. W. Hagen, M. Lebois, J. Lei, V. Méot, B. Morillon, A. M. Moro, T. Renstrøm, O. Roig, S. J. Rose, O. Sérot, S. Siem, I. Tsekhanovich, G. M. Tveten, M. Wiedeking, Investigation of the ^{238}U(d,p) surrogate reaction via the simultaneous measurement of γ-decay and fission probabilities, Phys. Rev. C **94**, 024614 (2016).
[14] H. C. Britt and J. D. Cramer, Fission of Odd-A Uranium and Plutonium Isotopes Excited by (d,p), (t,d), and (t,p) Reactions, Phys. Rev. C **2**, 1758 (1970).
[15] G. Kessedjian, B. Jurado, M. Aiche, G. Barreau, A. Bidaud, S. Czajkowski, D. Dassié, B. Haas, L. Mathieu, L. Audouin, N. Capellan, L. Tassan-Got, J. N. Wilson, E. Berthoumieux, F. Gunsing, Ch. Theisen, O. Sérot, E. Bauge, I. Ahmad, J. P. Greene and R. V. F. Janssens, Neutron-induced fission cross sections of short-lived actinides with the surrogate reaction method, Phys. Lett. B **692**, 297 (2010).
[16] D. Ramos, M. Caamaño, A. Lemasson, M. Rejmund, L. Audouin, H. Álvarez-Pol, J. D. Frankland,

B. Fernández-Domínguez, E. Galiana-Baldó, J. Piot, D. Ackermann, S. Biswas, E. Clement, D. Durand, F. Farget, M. O. Fregeau, D. Galaviz, A. Heinz, A. I. Henriques, B. Jacquot, B. Jurado, Y. H. Kim, P. Morfouace, D. Ralet, T. Roger, C. Schmitt, P. Teubig, and I. Tsekhanovich, First Direct Measurement of Isotopic Fission-Fragment Yields of ^{239}U, Phys. Rev. Lett. **123**, 092503 (2019).

[17] C. Rodríguez-Tajes, F. Farget, X. Derkx, M. Caamaño, O. Delaune, K.-H. Schmidt, E. Clément, A. Dijon, A. Heinz, T. Roger, L. Audouin, J. Benlliure, E. Casarejos, D. Cortina, D. Doré, B. Fernández-Domínguez, B. Jacquot, B. Jurado, A. Navin, C. Paradela, D. Ramos, P. Romain, M.D. Salsac, and C. Schmitt, Transfer reactions in inverse kinematics: An experimental approach for fission investigations, Phys. Rev. C **89**, 024614 (2014).

[18] R. Léguillon, K. Nishio, K. Hirose, H. Makii, I. Nishinaka, R. Orlandi, K. Tsukada, J. Smallcombe, S. Chiba, Y. Aritomo, T. Ohtsuki, R. Tatsuzawa, N. Takaki, N. Tamura, S. Goto, I. Tsekhanovich, C. M. Petrache and A. N. Andreyevand, Fission fragments mass distributions of nuclei populated by the multinucleon transfer channels of the ^{18}O + ^{232}Th, Phys. Lett. B **761**, 125 (2016).

[19] M. Caamaño, O. Delaune, F. Farget, X. Derkx, K.-H. Schmidt, L. Audouin, C.-O. Bacri, G. Barreau, J. Benlliure, E. Casarejos, A. Chbihi, B. Fernández-Domínguez, L. Gaudefroy, C. Golabek, B. Jurado, A. Lemasson, A. Navin, M. Rejmund, T. Roger, A. Shrivastava, and C. Schmitt, Isotopic yield distributions of transfer-and fusion-induced fission from ^{238}U + ^{12}C reactions in inverse kinematics, Phys. Rev. C **88**, 024605 (2013).

[20] J. E. Escher, J. T. Harke, F. S. Dietrich, N. D. Scielzo, I. J. Thompson, W. Younes, Compound-nuclear reaction cross sections from surrogate measurements, Rev. Mod. Phys. **84**, 353 (2012).

[21] J. E. Escher, and F. S. Dietrich, Determining (n,f) cross sections for actinide nuclei indirectly: Examination of the surrogate ratio method, Phys. Rev. C **74**, 054601 (2006).

[22] S. Chiba and O. Iwamoto, Verification of the surrogate ratio method, Phys. Rev. C **81**, 044604 (2010).

[23] J. C. Lighthall, B. B. Back, S. I. Baker, S. J. Freeman, H. Y. Lee, B. P. Kay, S. T. Marley, K. E. Rehm, J. E. Rohrer, J. P. Schiffer, D. V. Shetty, A. W. Vann, J. R. Winkelbauer and A. H. Wuosmaa, Commissioning of the HELIOS spectrometer, Nucl. Instr. and Meth. A **622**, 97 (2010).

[24] P. T. MacGregor, D. K. Sharp, S. J. Freeman, C. R. Hoffman, B. P. Kay, T. L. Tang, L. P. Gaffney, E. F. Baader, M. J. G. Borge, P. A. Butler, W. N. Catford, B. D. Cropper, G. de Angelis, J. Konki, Th. Kröll, M. Labiche, I. H. Lazarus, R. S. Lubna, I. Martel, D. G. McNeel, R. D. Page, O. Poleshchuk, R. Raabe, F. Recchia and J. Yang, Evolution of single-particle structure near the N = 20 island of inversion, Phys. Rev. C **104**, L051301 (2021).

[25] SOLARIS White Paper, Argonne National Laboratory, anl.gov/reference/solaris-white-paper.

[26] frib.msu.edu.

[27] lisa-itn.web.cern.ch.

[28] C. R. Gruhn, M. Binimi, R. Legrain, R. Loveman, W. Pang, M. Roach, D. K. Scott, A. Shotter, T. J. Symons, J. Wouters, M. Zisman, R. Devries, Y. C. Peng and W. Sondheim, Bragg curve spectroscopy, Nucl. Instr. and Meth. **196**, 33 (1982).

[29] The reaction Q value, and the hence excitation energy of the residual nucleus, is deduced from the calculated c.m. energy of the outgoing proton $E_{\rm cm}$. This is, in turn, related to the measured laboratory proton energy $E_{\rm lab}$ and the distance z travelled by the proton before returning to the beam axis via $E_{\rm cm} = E_{\rm lab} + \frac{m}{2}V_{\rm cm}^2 - \frac{mV_{\rm cm}z}{T_{\rm cyc}}$, where m is the proton mass, $V_{\rm cm}$ is the known c.m. velocity of the beam, and $T_{\rm cyc}$ is the cyclotron period of the proton. This is detailed in A. H. Wuosmaa, J. P. Schiffer, B. B. Back, C. J. Lister and K. E. Rehm, A solenoidal spectrometer for reactions in inverse kinematics, Nucl. Instr. and Meth. A **580**, 1290 (2007).

[30] S. Bjørnholm and J. E. Lynn, The double-humped fission barrier, Rev. Mod. Phys. **52**, 725 (1980).

[31] K.-H. Schmidt, B. Jurado, C. Amouroux, and Ch. Schmitt, General description of fission observables: GEF model code, Nuclear Data Sheets **131**, 107 (2016).

[32] A. J. M. Plompen, O. Cabellos, C. De Saint Jean, M. Fleming, *et al.*, The joint evaluated fission and fusion nuclear data library, JEFF-3.3, Eur. Phys. J A **56**, (2020).

[33] D. A. Brown, M. B. Chadwick, R. Capote, A. C. Kahler, A. Trkov, M. W. Herman, A. A. Sonzogni, Y. Danon, A. D. Carlson, M. Dunn *et al.*, ENDF/B-VIII.0: The 8th major release of the nuclear reaction data library with CIELO-project cross sections, new standards and thermal scattering data, Nuclear Data Sheets **148**, 1 (2018).

[34] K. Shibata, O. Iwamoto, T. Nakagawa, N. Iwamoto, A. Ichihara, S. Kunieda, S. Chiba, K. Furutaka, N. Otuka, T. Ohsawa *et al.*, JENDL-4.0: a new library for nuclear science and engineering, Journal of Nuclear Science and Technology **48**, 1 (2011).

[35] A. Pal, S. Santra, D. Chattopadhyay, A. Kundu, K. Ramachandran, R. Tripathi, B. J. Roy, T. N. Nag, Y. Sawant, and D. Sarkar, Projectile-breakup-induced fission-fragment angular distributions in the ^{6}Li + ^{232}Th reaction, Phys. Rev. C **96**, 024603 (2017).

[36] Supplemental Material are available at [URL to be submitted by publisher].

[37] The data and associated information are available at doi.org/10.5281/zenodo.7303765.